



# NIH Public Access

## Author Manuscript

*Nat Chem.* Author manuscript; available in PMC 2013 August 01.

Published in final edited form as:  
*Nat Chem.* ; 4(8): 615–620. doi:10.1038/nchem.1375.

## Crystal structure of $\Delta$ -Ru(bpy)<sub>2</sub>dppz<sup>2+</sup> bound to mismatched DNA reveals side-by-side metalloinsertion and intercalation

Hang Song, Jens T. Kaiser, and Jacqueline K. Barton\*

Division of Chemistry and Chemical Engineering California Institute of Technology Pasadena, CA 91125

### Abstract

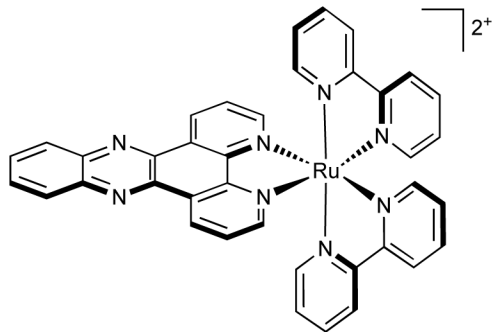
DNA mismatches represent a novel target in developing diagnostics and therapeutics for cancer, since deficiencies in DNA-mismatch repair (MMR) are implicated in many cancers and cells that are MMR-deficient show a high frequency of mismatches. We use metal complexes with bulky intercalating ligands serve as probes for DNA mismatches. Here, we report the high resolution (0.92 Å) crystal structure of the ruthenium ‘light switch’ complex  $\Delta$ -Ru(bpy)<sub>2</sub>dppz<sup>2+</sup> (bpy = 2,2'-bipyridine and dppz = dipyridophenazine), known to show luminescence on binding to duplex DNA, bound to both mismatched and well matched sites in the oligonucleotide 5'-(dCGGAAATTACCG)<sub>2</sub>-3' (underline denotes AA mismatches). Two crystallographically independent views reveal that the complex binds mismatches through metalloinsertion, where the dppz inserts into the duplex through the minor groove, ejecting both mispaired adenosines. Additional ruthenium complexes are intercalated at well-matched sites, creating an array of complexes in the minor groove stabilized through stacking interactions between bpy ligands and extruded adenosines. This structure attests to the generality of metalloinsertion and metallointercalation as DNA binding modes.

Deficiencies in DNA mismatch repair (MMR) have been linked to increased rate of mutation and several types of cancers.<sup>1–7</sup> Detection of MMR deficiency typically relies on assessment of markers for microsatellite instability, promoter hypermethylation and/or immunohistological staining of MMR proteins.<sup>8–10</sup> These methods may not be applicable to all cancers, and more than one MMR protein needs to be considered. On the other hand, all forms of MMR deficiency are expected to show elevated levels of DNA mismatches, which by themselves would be a persistent and universal target for diagnostic agents. Luminescent, mismatch-targeting small molecules are thus ideally suited to become a direct, fast, and sensitive detection method for MMR deficiency in biological samples. We have previously discovered that the metal complex Ru(bpy)<sub>2</sub>dppz<sup>2+</sup> (where bpy = 2,2'-bipyridine and dppz = dipyrido[3,2-*a*:2',3'-*c*]phenazine) shows enhanced luminescence in the presence of base mismatches and abasic sites.<sup>11</sup> Its augmented luminescence sensitivity to mismatches makes it a promising parent complex for the design of luminescence-based mismatch sensors. Further development necessitates a thorough structural understanding of the interactions between the ruthenium complex and DNA. Here, we report the atomic resolution structure of  $\Delta$ -Ru(bpy)<sub>2</sub>dppz<sup>2+</sup> (**1**) cocrystallized with a 12-mer oligonucleotide containing two adenine-adenosine mismatches, and examine in detail the binding interactions between the metal complex and DNA.

\*To whom correspondence should be addressed at jkbarton@caltech.edu.

**AUTHOR CONTRIBUTIONS** J.K.B. and H.S. designed the research. H.S. carried out crystallization and solution luminescence experiments. J.T.K. and H.S. solved the crystal structure. H.S. and J.K.B. wrote the manuscript.

**COMPETING FINANCIAL INTERESTS** The authors declare no competing financial interests.



Dppz complexes of ruthenium have been widely studied due to their unique photophysical responses to DNA. Typically, emission from these complexes is extremely weak in water, but their luminescence is significantly enhanced upon binding to double-stranded DNA, hence the “light switch” effect.<sup>12</sup> Extensive studies in solution have established that these complexes bind to DNA by intercalation through the planar dppz ligand.<sup>13-17</sup> Some possible structures have been put forward through theoretical calculations;<sup>18-19</sup> however, due to the lack of site-specificity in DNA binding, solution and crystal structures have largely remained elusive. Although the discovery of the unique photophysical properties of this class of complexes was made over two decades ago, the first crystal structure of a dppz complex bound to DNA was not obtained until very recently, but it did not capture dppz intercalation into a native DNA duplex.<sup>20</sup>

Besides binding to well-matched DNA, Ru(bpy)<sub>2</sub>dppz<sup>2+</sup> shows further enhanced luminescence in the presence of DNA defects such as base mismatches.<sup>11</sup> We have proposed that the binding of Ru(bpy)<sub>2</sub>dppz<sup>2+</sup> to mismatches occurs by metalloinsertion.<sup>11</sup> This binding mode has been elucidated in crystal structures of the mismatch-targeting rhodium complex,  $\Delta$ -Rh(bpy)<sub>2</sub>chrysi<sup>3+</sup> (where chrysi = chrysene-5,6-quinone diimine), bound to an AC or AA mismatch, as well as in solution NMR studies with a CC mismatch.<sup>21-24</sup> In this binding mode, the intercalating chrysi ligand inserts into the mismatch site from the minor groove and extrudes the mispaired bases out of the helix, effectively taking their place in the base stack. Here we show that in the ruthenium-DNA crystal structure, just like the rhodium complex, Ru(bpy)<sub>2</sub>dppz<sup>2+</sup> binds to mismatches also through metalloinsertion, the inserting ligand is dppz. The crystal structure described herein, at 0.92-Å resolution, provides several independent views of ruthenium binding to DNA through dppz intercalation and insertion, illustrating the structural basis of the interactions between DNA and the “light switch” molecule as captured by cocrystallization.

## RESULTS AND DISCUSSION

### Cocrystallization of $\Delta$ -Ru(bpy)<sub>2</sub>dppz<sup>2+</sup> with DNA

To elucidate the structural basis for Ru(bpy)<sub>2</sub>dppz<sup>2+</sup> interaction with DNA, we cocrystallized  $\Delta$ -Ru(bpy)<sub>2</sub>dppz<sup>2+</sup> (**1**) with the 12-mer palindromic DNA sequence, d(C<sub>1</sub>G<sub>2</sub>G<sub>3</sub>A<sub>4</sub>A<sub>5</sub>A<sub>6</sub>T<sub>7</sub>T<sub>8</sub>A<sub>9</sub>C<sub>10</sub>C<sub>11</sub>G<sub>12</sub>)<sub>2</sub>. This sequence contains two AA mismatches (underlined) and has been previously cocrystallized with  $\Delta$ -Rh(bpy)<sub>2</sub>chrysi<sup>3+</sup>.<sup>22</sup> We considered that similar binding of the complex at the mismatched site might yield well defined crystals. Crystals took longer than two months to appear in the crystallization wells, however. The metal complex and the oligonucleotide cocrystallized in space group *P*1 (see Supplementary Table S1 for data collection and refinement statistics). The asymmetric unit contains one double strand of DNA with five bound ruthenium complexes. The structure, at atomic resolution, revealed three binding modes of the ruthenium complex: (i) metalloinsertion at the mismatched sites with ejection of the mispaired adenosines, (ii)

metallointercalation between well-matched base pairs and (iii) end-capping between two (crystallographically-related) duplexes (Figure 1).

### Metalloinsertion at mismatched sites

At the two destabilized AA mismatches, the metal complex inserts deeply from the minor groove and fully ejects the mispaired adenosines (Figure 1 and Supplementary Figure S1). We had proposed that Ru(bpy)<sub>2</sub>dppz<sup>2+</sup> binds to DNA mismatches through insertion from the minor groove, and that metalloinsertion may be a general binding mode for octahedral metal complexes bearing planar ligands.<sup>11</sup> Increased luminescence is found with a range of DNA mismatches, and, as with the Rh complexes, correlates with thermodynamic instability of the mismatch. Here, consistent with our proposal, the ruthenium complex indeed binds tightly to both mismatched sites through metalloinsertion, with the dppz ligand stacked between the two flanking base pairs, effectively replacing the mispaired adenosines in the base stack. All four ejected adenosines are folded back in the minor groove. They adopt the *syn* conformation and stack with the very ruthenium that is inserted at their respective mismatched site. An overlay of the two separate metalloinsertion sites shows that the local geometry of the DNA and the relative orientation of the ruthenium complex are highly conserved between the two sites (Figure 2). The dppz is inserted in a head-on fashion, positioned halfway between the phosphate backbones, both phenazine nitrogens are well protected from solvent access. On the other hand, if we only consider the relative orientation of the dppz with respect to the base pairs above and below the insertion site, the dppz is inserted at an angle with respect to the dyad axis of either flanking base pair. Compared to the chrysyl ligand, dppz is narrower and symmetric about its long axis. As a result, while the DNA minor groove widens significantly in the rhodium structures to accommodate the sterically expansive and asymmetric chrysyl complex,<sup>21,22</sup> it does so to a lesser extent in the case of the ruthenium complex (Supplementary Figure S2).

### Intercalation at matched sites

Of the three remaining ruthenium complexes, two are intercalated between well-matched base pairs, also through the minor groove. This mode of intercalation, namely from the minor groove, contrasts what was inferred from NMR and competitive fluorescence studies, in which we had deduced a major groove preference for metallointercalation;<sup>14,17,25</sup> linear dichroism studies did, however, suggest minor groove association<sup>15,16</sup>. We note that in this structure, intercalation occurs in conjunction with stacking interactions between an ancillary bpy ligand of the intercalating complex and either an extruded adenosine or a bpy ligand from a neighboring complex. These stacking interactions serve to stabilize the intercalated complex in the minor groove. These contrasting results indicate that the energetic difference between intercalation from the major groove versus the minor groove must be small. Computational studies of dppz complexes intercalated into a dinucleotide step also support the notion of very small differences in intercalation energetics from the two grooves.<sup>18</sup> In this intercalative binding mode, the dppz ligand is positioned inside the base stack also in a head-on fashion. The intercalation of the dppz ligand is so deep that the end most distal from the ruthenium center protrudes into the major groove. Comparison between the two independent intercalation sites reveals subtle differences in the relative position of the complex (Figure 3). In the 5'-A<sub>6</sub>T<sub>7</sub>-3' step, the dppz is right in the middle of the two strands and intercalated more deeply, with most of the stacking interactions formed between the central ring of the phenazine portion and the bases. For the 5'-C<sub>1</sub>G<sub>2</sub>-3' step, the dppz is closer to one strand than the other, and both the distal and the central rings of the phenazine are involved in stacking.

## Crystal packing

The fifth ruthenium complex is sandwiched between two crystallographically related duplexes (Figure 4). The last GC base pair becomes a frayed end, with the cytidine and the guanosine pointing down into the minor and major groove of the next duplex, respectively. The dppz ligand of the end-capping ruthenium complex effectively replaces this terminal base pair in the helix, providing an anchor for the next duplex to stack upon.

## Local distortions of the oligonucleotide duplex

在整个DNA螺旋中，小沟是密集地由交替的金属复合物和挤出的腺嘌呤核苷酸占据的。五个金属复合物均匀地间隔，结合到DNA上，每隔两个碱基对。四个错配的腺嘌呤核苷酸被五个金属复合物夹在中间，最后一个金属复合物与下一个重复单元中的第一个金属复合物接触。DNA保持其B型形式，尽管有一些局部偏差从理想的B型几何学（表1和补充表S2）出发。整体结构稍微向大沟弯曲，类似于我们在相同的DNA序列中观察到的铑结构。<sup>22</sup>所有碱基对都显示一些程度的解旋以适应插入和间插的复合物（表1），正如预期的那样，因为DNA的解旋通常与间插剂相关。<sup>26-28</sup>大多数糖环都是C2'-endo或与之密切相关的C1'-exo（或C3'-exo，补充表S2），表明交替的C2'-endo/C3'-endo构象<sup>26</sup>不是必要的。上升高度在每个钌结合位点处大约加倍，因为金属复合物作为额外的碱基对在螺旋中起作用，但有趣的是，相邻的天然碱基对之间的上升高度少于3.3 Å（表1）。这种垂直空间压缩可能是一个指示信号，表明在bpy配体和挤出的腺嘌呤核苷酸之间存在堆叠，使得间隔位点的碱基对必须缩短它们的上升高度以使bpy和腺嘌呤核苷酸能够接触。平均距离bpy和腺嘌呤核苷酸实际上为3.3 Å。这与我们的观点一致，即腺嘌呤-bpy堆叠可能是驱动钌的间插作用的小沟。但重要的是，腺嘌呤核苷酸在第一次插入时被挤出，因为钌复合物插入在错配位点，且金属插入通常通过小沟显而易见。<sup>21,22</sup>

## Comparison with other structures

第一个dppz复合物与DNA结合的晶体结构是λ-对映体的Ru(TAP)<sub>2</sub>dppz<sup>2+</sup>（TAP = 1,4,5,8-tetraazaphenanthrene）与一个10-mer寡核苷酸结合的。<sup>20</sup>钌复合物通过半间插作用于TAP配体，该配体介于两个GC碱基对之间，以及dppz配体介于一个GC碱基对和一个反Watson-Crick配对的AT碱基对之间，其中腺嘌呤和胸腺嘧啶来自对称相关的链。除了具有不同的辅助配体外，这个复合物与我们的钌复合物具有相反的手性。我们已经证明，在我们的结构中，Δ-异构体通过dppz配体在原生匹配碱基对之间进行间插，但在TAP结构中，这种结合模式不存在。这与早期的溶液研究表明，间插金属复合物结合到DNA上：辅助配体的λ-异构体将被右旋B型DNA的骨架 sterically排斥，而Δ-异构体具有正确的对称性以适应小沟。<sup>29</sup>在TAP结构中，DNA双链采用整体B型形式，尽管存在局部扭曲，且dppz间插仅发生在两个双链的接口处，而不是形成连续的螺旋。在

same time, the semi-intercalation of TAP induces a severe kink in the DNA. For the TAP ligand, full intercalation from the minor groove may be more difficult for the  $\lambda$ -configuration. With bpy ligands metalloinsertion is highly favored for the  $\Delta$ -isomer, but only small enantiomeric discrimination occurs with intercalation.<sup>24</sup> Indeed, the  $\Delta$ -isomer, as shown in the structure reported herein, binds avidly to the right-handed helix through full intercalation. We may also compare our structure with that of  $\Delta$ -Rh(Me<sub>2</sub>trien)phi<sup>3+</sup> (Me<sub>2</sub>trien = 2*R*,9*R*-diamino-4,7-diazadecane) intercalated in an 8-mer oligonucleotide.<sup>27</sup> The rhodium structure shows only one complex bound per 8-mer duplex, as opposed to five ruthenium molecules per 12-mer duplex in our structure. Functional groups were installed on the rhodium complex to form sequence-specific contacts with the DNA in the major groove, hence the single-site binding at a specific step in the base stack. The complex Ru(bpy)<sub>2</sub>dppz<sup>2+</sup>, on the other hand, binds nonspecifically to DNA. Thus, binding at multiple sites along the duplex is observed in the ruthenium structure. The sequence context of the intercalation or insertion sites – pyrimidine-purine (5'-C<sub>1</sub>G<sub>2</sub>-3'), pyrimidine-pyrimidine (5'-T<sub>8</sub>C<sub>10</sub>-3'), purine-purine (5'-G<sub>3</sub>A<sub>5</sub>-3'), and purine-pyrimidine (5'-A<sub>6</sub>T<sub>7</sub>-3') – also speaks to the non-specific nature of DNA binding by the ruthenium complex.

### Solution luminescence

We measured the solution luminescence of  $\Delta$ -Ru(bpy)<sub>2</sub>dppz<sup>2+</sup> (**1**) bound to the mismatched oligonucleotide, as well as to a fully complementary 12-mer oligonucleotide d(CGGTAATTACCG)<sub>2</sub>, in order to determine if the crystal structure reflects binding preferences in solution. As the AA mismatch-containing duplex has a low melting temperature of 22°C, the experiments were conducted at 4°C to ensure all DNA strands are properly hybridized. The luminescence from  $\Delta$ -Ru(bpy)<sub>2</sub>dppz<sup>2+</sup> (**1**) bound to mismatched DNA is about three times the luminescence with the equivalent 12-mer well-matched duplex (Figure 5), consistent with previously observed higher sensitivity of Ru(bpy)<sub>2</sub>dppz<sup>2+</sup> luminescence response to mismatched DNA.

To determine the groove preference of ruthenium complex binding, we employed the minor groove-specific quencher, Cu(phen)<sub>2</sub><sup>2+</sup>,<sup>30,31</sup> to quench the luminescence from the ruthenium complex (Figure 5). Quenching by paramagnetic Cu(phen)<sub>2</sub><sup>2+</sup> is expected rather than a direct competition for binding sites; Cu(phen)<sub>2</sub><sup>2+</sup>, a non-specific groove binder, binds several orders of magnitude more weakly to DNA than the intercalative ruthenium complex. The luminescence associated with mismatched DNA is significantly quenched (by 34%) with increasing concentrations of Cu(phen)<sub>2</sub><sup>2+</sup>, while luminescence associated with the matched sequence is quenched to a much lesser extent (12%). This differential quenching is consistent with the mismatch-bound ruthenium complexes being located in the minor groove, but those bound to well-matched DNA are mostly in the major groove. Therefore, although the crystal structure provides a very detailed picture of metalloinsertion and metallointercalation in the minor groove, it may not capture intercalation events occurring in the major groove. Perhaps the inherently dynamic nature of ruthenium intercalation from the major groove, as reflected in the fast exchange and multiple binding conformations revealed in NMR studies, hinders the formation of well-packed crystals. Nonetheless, the crystal structure still provides invaluable insight into intercalation of  $\Delta$ -Ru(bpy)<sub>2</sub>dppz<sup>2+</sup> (**1**) when it is in the minor groove.

## CONCLUSIONS

The structure presented here at 0.92 Å-resolution depicts in detail the versatile binding modes attainable for octahedral metal complexes bearing an intercalating ligand. It shows two independent views of metalloinsertion, two of intercalation, and one of end-capping. At destabilized regions of the DNA, the metal complex binds through metalloinsertion in the

minor groove, accompanied by extrusion of the mismatched bases. This binding mode was previously observed with a sterically expansive ligand, but this structure clearly demonstrates that a narrower ligand such as dppz is equally capable of recognizing mismatches by metalloinsertion, pointing to the generality of this binding mode. The smaller size of the dppz ligand allows the ruthenium complex also to bind through classical intercalation between two consecutive well-matched base pairs. Curiously, intercalated complexes are located in the minor groove as well, which we hypothesize is stabilized by extensive ancillary interactions; given some major groove intercalation in solution, binding from the major and minor groove must be energetically similar. This discrepancy notwithstanding, the crystal structure attests to the remarkable structural flexibility of DNA upon high-density ligand binding, illustrates the nuanced binding geometries sampled by a non-covalently bound small molecule, and highlight the dominance of metalloinsertion as the preferred binding mode to destabilized regions of DNA. We hope these newly garnered structural understandings will help guide the development of future generations of metal complexes as chemical tools and medicinal agents.

## METHODS

### Materials

[Ru(bpy)<sub>2</sub>dppz]Cl<sub>2</sub> was synthesized according to previously reported procedures.<sup>32</sup> The enantiomers were separated using a CYCLOBOND I 2000 DMP HPLC column (Sigma) on a Hewlett-Packard 1100 HPLC, with an isocratic solvent composition of 60/40 (v/v) CH<sub>3</sub>CN:100 mM KPF<sub>6</sub> (aq). The Δ-enantiomer eluted first, followed by the λ-isomer. The assignment of the two fractions was confirmed by circular dichroism.<sup>33</sup> The fractions were lyophilized and washed with water to remove excess KPF<sub>6</sub> and exchanged for chloride salt on a QAE anion-exchange column. Oligonucleotides (Integrated DNA Technologies) were purified by reverse-phase HPLC using a C18 reverse-phase column (Varian) on a Hewlett-Packard 1100 HPLC. Quantification was performed on a Beckman DU 7400 spectrophotometer.

### Crystallization and data collection

Oligonucleotides were incubated with Δ-[Ru(bpy)<sub>2</sub>dppz]Cl<sub>2</sub> (**1**) before crystallization. Subsequent manipulations were performed with minimal exposure of the complex to light. The crystal was grown from a solution of 1 mM d(C<sub>1</sub>G<sub>2</sub>G<sub>3</sub>A<sub>4</sub>A<sub>5</sub>A<sub>6</sub>T<sub>7</sub>T<sub>8</sub>A<sub>9</sub>C<sub>10</sub>C<sub>11</sub>G<sub>12</sub>)<sub>2</sub>, 2 or 3 mM enantiomerically pure Δ-Ru(bpy)<sub>2</sub>dppz<sup>2+</sup> (**1**), 20 mM sodium cacodylate (pH 7.0), 6 mM sperminetetrahydrochloride, 40 mM NaCl or KCl, 10 mM BaCl<sub>2</sub>, and 5% 2-methyl-2,4-pentanediol (MPD) equilibrated in sitting drops versus a reservoir of 35% MPD at ambient temperature. The crystals grew in space group *P*1 and unit cell dimensions: *a* = 24.039 Å, *b* = 24.797 Å, *c* = 37.521 Å,  $\alpha$  = 74.669°,  $\beta$  = 84.416°, and  $\gamma$  = 76.208° (Supplementary Table S1).

Data were collected from a flash-cooled crystal at 100 K on an R-axis IV image plate using Cu Kα radiation produced by a Rigaku RU-H3RHB rotating-anode generator with double-focusing mirrors and a Ni filter. High-resolution data were subsequently collected from a different crystal on beamline 12-2 at the Stanford Synchrotron Radiation Laboratory (Menlo Park, CA,  $\lambda$  = 0.7749 Å, 100 K, PILATUS 6M detector). The data were processed with or XDS<sup>34</sup>, and SCALA from the CCP4 suite of programs.<sup>35</sup>

### Structure determination and refinement

The structure was determined by single anomalous dispersion phasing using the anomalous scattering of ruthenium with the Shelxc/d/e suite of programs.<sup>36</sup> Five heavy atoms were located per asymmetric unit. The model was built in COOT<sup>37</sup> and refined with PHENIX

version 1.7.<sup>38</sup> The anomalous contribution of ruthenium was taken into account and alternative conformations of phosphates were included in the refinement. Atomic displacement factors have been refined anisotropically. Figures were drawn with Pymol.<sup>39</sup> Alignment was performed with LSQMAN.<sup>40</sup> The coordinates and structure factors have been deposited in RCSB Protein Data Bank (PDB ID: 4E1U).

### Steady state fluorescence

Luminescence spectra (excitation wavelength = 440 nm) with emission intensities ranged from 560 to 800 nm were measured in 40 mM sodium cacodylate (pH 7.0), 80 mM KCl, 20 mM BaCl<sub>2</sub> on an ISS-K2 spectrophotometer at 4°C in aerated solutions. Cu(phen)<sub>2</sub><sup>2+</sup> was formed in situ using 1:3 CuCl<sub>2</sub> and phenanthroline. Experiments were performed in triplicate.

## Supplementary Material

Refer to Web version on PubMed Central for supplementary material.

### Acknowledgments

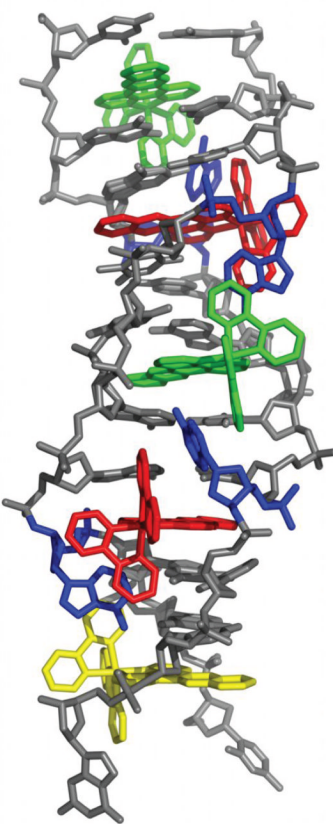
We thank S. C. Virgil for assistance in the separation of enantiomers, and D. C. Rees and J. A. Hoy for valuable discussions. We are grateful to the National Institutes of Health (NIH GM33309 to J. K. B.) for their financial support and the Tobacco-Related Disease Research Program (TRDRP) for a Dissertation Research Award to H. S. We acknowledge the Gordon and Betty Moore Foundation and Sanofi-Aventis Bioengineering Research Program at Caltech for support of the X-ray Facility at the Caltech Molecular Observatory. The rotation camera facility at Stanford Synchrotron Radiation Laboratory is supported by the U.S. Department of Energy and NIH.

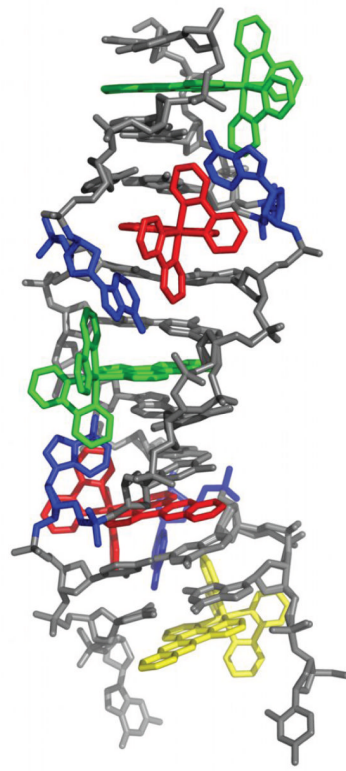
## REFERENCES

1. Loeb LA. A mutator phenotype in cancer. *Cancer Res.* 2001; 61:3230–3239. [PubMed: 11309271]
2. Strauss BS. Frameshift mutation, microsatellites and mismatch repair. *Mutat. Res.* 1999; 437:195–203. [PubMed: 10592327]
3. Papadopoulos N, Lindblom A. Molecular basis of HNPCC: mutations of MMR genes. *Hum. Mutat.* 1997; 10:89–99. [PubMed: 9259192]
4. Peltomaki P. Deficient DNA mismatch repair: a common etiologic factor for colon cancer. *Hum. Mol. Genet.* 2001; 10:735–740. [PubMed: 11257106]
5. Lawes DA, SenGupta S, Boulos PB. The clinical importance and prognostic implications of microsatellite instability in sporadic cancer. *Eur. J. Surg. Oncol.* 2003; 29:201–212. [PubMed: 12657227]
6. Bhattacharyya NP, Skandalis A, Ganesh A, Groden J, Meuth M. Mutator phenotypes in human colorectal carcinoma cell lines. *Proc. Natl. Acad. Sci. USA.* 1994; 91:6319–6323. [PubMed: 8022779]
7. Arzimanoglou II, Gilbert F, Barber HRK. Microsatellite instability in human solid tumors. *Cancer.* 1998; 82:1808–1820. [PubMed: 9587112]
8. Boland CR, et al. A national cancer institute workshop on microsatellite instability for cancer detection and familial predisposition: development of international criteria for the determination of microsatellite instability in colorectal cancer. *Cancer Res.* 1998; 58:5248–5257. [PubMed: 9823339]
9. de la Chapelle A. Microsatellite instability. *N. Engl. J. Med.* 2003; 349:209–210. [PubMed: 12867603]
10. Rosen DG, Cai KQ, Luthra R, Liu J. Immunohistochemical staining of hMLH1 and hMSH2 reflects microsatellite instability status in ovarian carcinoma. *Mod Pathol.* 2006; 19:1414–1420. [PubMed: 16941012]
11. Lim MH, Song H, Olmon ED, Dervan EE, Barton JK. Sensitivity of Ru(bpy)<sub>2</sub>dppz<sup>2+</sup> luminescence to DNA defects. *Inorg. Chem.* 2009; 48:5392–5397. [PubMed: 19453124]

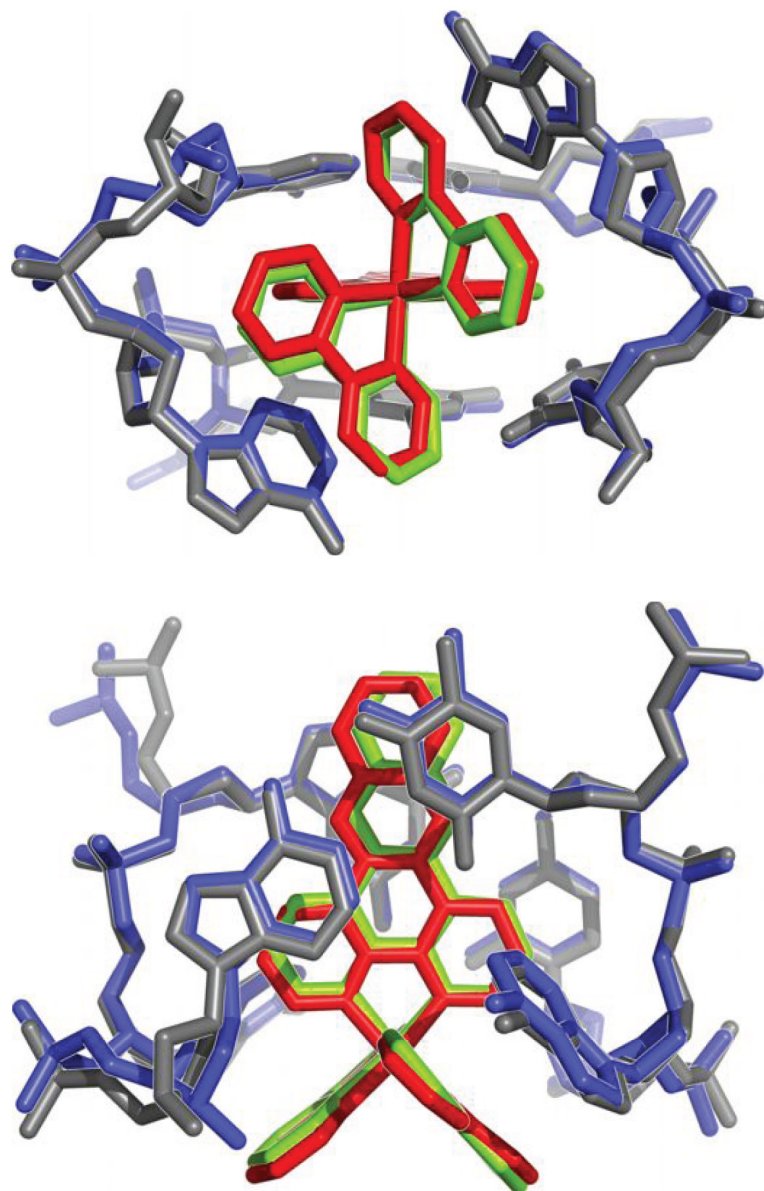
12. Friedman AE, Chambron JC, Sauvage JP, Turro NJ, Barton JK. A molecular light switch for DNA: Ru(bpy)<sub>2</sub>(dppz)<sup>2+</sup>. *J. Am. Chem. Soc.* 1990; 112:4960–4962.
13. Hiort C, Lincoln P, Norden B. DNA binding of Δ- and λ-[Ru(phen)<sub>2</sub>DPPZ]<sup>2+</sup>. *J. Am. Chem. Soc.* 1993; 115:3448–3454.
14. Dupureur CM, Barton JK. Use of selective deuteration and <sup>1</sup>H NMR in demonstrating major groove binding of Δ-[Ru(phen)<sub>2</sub>dppz]<sup>2+</sup> to d(GTCGAC)<sub>2</sub>. *J. Am. Chem. Soc.* 1994; 116:10286–10287.
15. Haq I, et al. Interaction of Δ- and λ-[Ru(phen)<sub>2</sub>DPPZ]<sup>2+</sup> with DNA: a calorimetric and equilibrium binding study. *J. Am. Chem. Soc.* 1995; 117:4788–4796.
16. Lincoln P, Broo A, Norden B. Diastereomeric DNA-binding geometries of intercalated ruthenium(II) trischelates probed by linear dichroism: [Ru(phen)<sub>2</sub>DPPZ]<sup>2+</sup> and [Ru(phen)<sub>2</sub>BDPPZ]<sup>2+</sup>. *J. Am. Chem. Soc.* 1996; 118:2644–2653.
17. Dupureur CM, Barton JK. Structural studies of λ- and Δ-[Ru(phen)<sub>2</sub>dppz]<sup>2+</sup> bound to d(GTCGAC)<sub>2</sub>: characterization of enantioselective intercalation. *Inorg. Chem.* 1997; 36:33–43.
18. Ambrosek D, Loos P-F, Assfeld X, Daniel C. A theoretical study of Ru(II) polypyridyl DNA intercalators: structure and electronic absorption spectroscopy of [Ru(phen)<sub>2</sub>(dppz)]<sup>2+</sup> and [Ru(tap)<sub>2</sub>(dppz)]<sup>2+</sup> complexes intercalated in guanine–cytosine base pairs. *J. Inorg. Biochem.* 2010; 104:893–901. [PubMed: 20554006]
19. Vargiu AV, Magistrato A. Detecting DNA mismatches with metallo-insertors: a molecular simulation study. *Inorg. Chem.* 2012; 51:2046–2057. [PubMed: 22288501]
20. Hall JP, et al. Structure determination of an intercalating ruthenium dipyridophenazine complex which kinks DNA by semiintercalation of a tetraazaphenanthrene ligand. *Proc. Natl Acad. Sci. USA.* 2011; 108:17610–17614. [PubMed: 21969542]
21. Pierre VC, Kaiser JT, Barton JK. Insights into finding a mismatch through the structure of a mispaired DNA bound by a rhodium intercalator. *Proc. Natl Acad. Sci. USA.* 2007; 104:429–434. [PubMed: 17194756]
22. Zeglis BM, Pierre VC, Kaiser JT, Barton JK. A bulky rhodium complex bound to an adenosine–adenosine DNA mismatch: general architecture of the metalloinsertion binding mode. *Biochemistry.* 2009; 48:4247–4253. [PubMed: 19374348]
23. Cordier C, Pierre VC, Barton JK. Insertion of a bulky rhodium complex into a DNA cytosine–cytosine mismatch: an NMR solution study. *J. Am. Chem. Soc.* 2007; 129:12287–12295. [PubMed: 17877349]
24. Zeglis BM, Pierre VC, Barton JK. Metallo-intercalators and metallo-insertors. *Chem. Commun. (Camb.).* 2007; 44:4565–4579. [PubMed: 17989802]
25. Holmlin RE, Stemp EDA, Barton JK. Ru(phen)<sub>2</sub>dppz<sup>2+</sup> luminescence: dependence on DNA sequences and groove-binding agents. *Inorg. Chem.* 1998; 37:29–34. [PubMed: 11670256]
26. Sobell HM, Tsai C-C, Jain SC, Gilbert SG. Visualization of drug-nucleic acid interactions at atomic resolution: III. Unifying structural concepts in understanding drug-DNA interactions and their broader implications in understanding protein-DNA interactions. *J. Mol. Biol.* 1977; 114:333–365. [PubMed: 71352]
27. Kielkopf CL, Erkkila KE, Hudson BP, Barton JK, Rees DC. Structure of a photoactive rhodium complex intercalated into DNA. *Nat. Struct. Mol. Biol.* 2000; 7:117–121.
28. Adams A, Guss JM, Denny WA, Wakelin LPG. Crystal structure of 9-amino-N-[2-(4-morpholinyl)ethyl]-4-acridinecarboxamide bound to d(CGTACG)<sub>2</sub>: implications for structure–activity relationships of acridinecarboxamide topoisomerase poisons. *Nucleic Acids Res.* 2002; 30:719–725. [PubMed: 11809884]
29. Barton JK. Metals and DNA: molecular left-handed complements. *Science.* 1986; 233:727–734. [PubMed: 3016894]
30. Sigman DS, Chen C-HB. Chemical nucleases: new reagents in molecular biology. *Annu. Rev. Biochem.* 1990; 59:207–236. [PubMed: 1695832]
31. Lim MH, Lau IH, Barton JK. DNA strand cleavage near a CC mismatch directed by a metalloinsertor. *Inorg. Chem.* 2007; 46:9528–9530. [PubMed: 17918931]

32. Amouyal E, Homsi A, Chambron J-C, Sauvage J-P. Synthesis and study of a mixed-ligand ruthenium(II) complex in its ground and excited states: bis(2,2'-bipyridine)(dipyrido[3,2-a:2',3'-c]phenazine-N<sup>4</sup>N<sup>5</sup>)ruthenium(II). *J. Chem. Soc., Dalton Trans.* 1990;1841–1845.
33. Liu J-G, et al. Enantiomeric ruthenium(II) complexes binding to DNA: binding modes and enantioselectivity. *J. Biol. Inorg. Chem.* 2000; 5:119–128. [PubMed: 10766444]
34. Kabsch W. XDS. *Acta Crystallogr. D.* 2010; 66:125–132. [PubMed: 20124692]
35. Collaborative Computational Project Number 4. The CCP4 suite: programs for protein crystallography. *Acta Crystallogr. D.* 1994; 50:760–763. [PubMed: 15299374]
36. Sheldrick GM. A short history of SHELX. *Acta Crystallogr. A.* 2008; 64:112–122. [PubMed: 18156677]
37. Emsley P, Cowtan K. Coot: model-building tools for molecular graphics. *Acta Crystallogr. D.* 2004; 60:2126–2132. [PubMed: 15572765]
38. Adams PD, et al. PHENIX: A comprehensive Python-based system for macromolecular structure solution. *Acta Crystallogr. D.* 2010; 66:213–221. [PubMed: 20124702]
39. Schrodinger, LLC. The PyMOL Molecular Graphics System. 2010.
40. Kleywegt GJ. Use of non-crystallographic symmetry in protein structure refinement. *Acta Crystallogr. D.* 1996; 52:842–857. [PubMed: 15299650]
41. Lu X, Olson WK. DNA: a software package for the analysis, rebuilding and visualization of three-dimensional nucleic acid structures. *Nucleic Acids Res.* 2003; 31:5108–5121. [PubMed: 12930962]

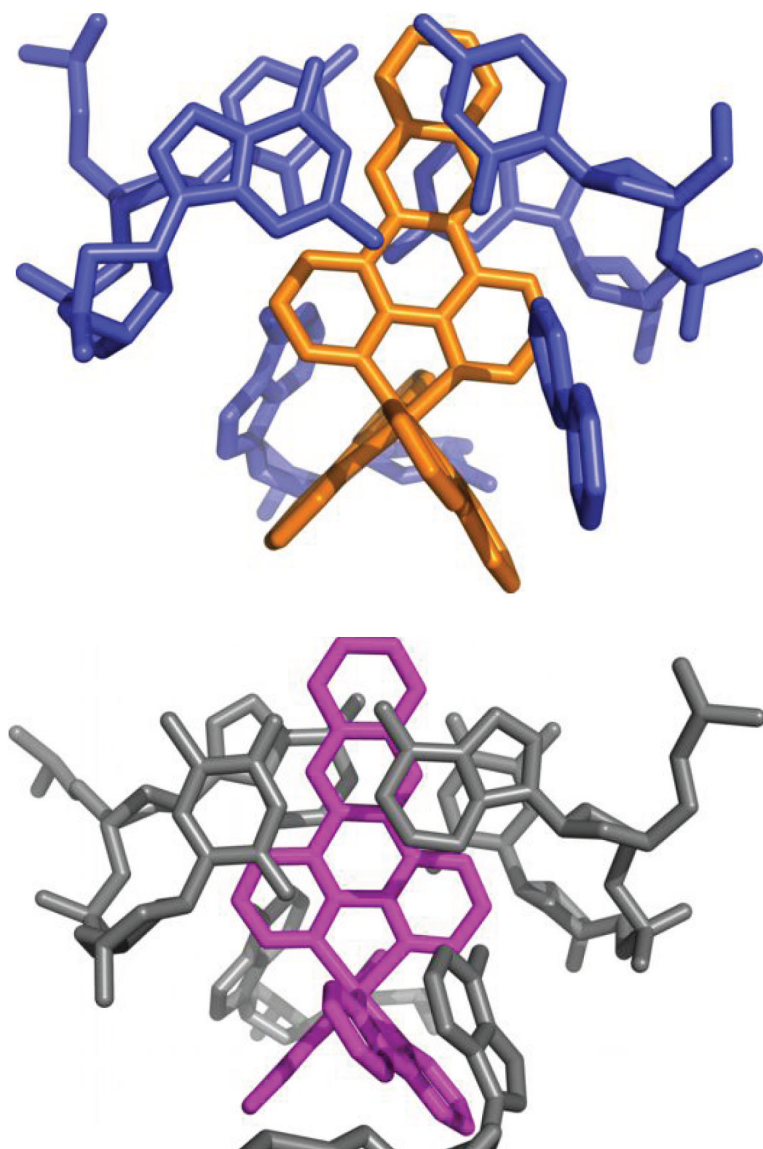


**Figure 1.**

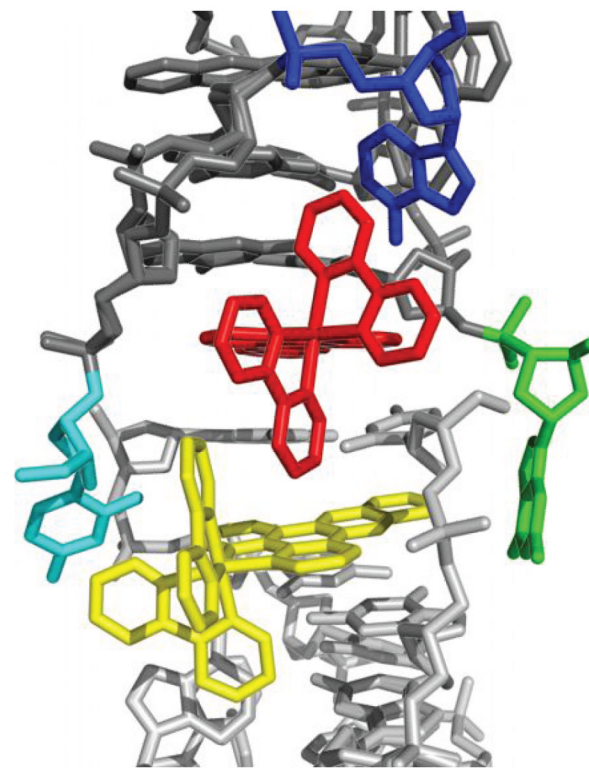
Structure of  $\Delta\text{-Ru}(\text{bpy})_2\text{dppz}^{2+}$  (1) bound to the oligonucleotide 5'-C<sub>1</sub>G<sub>2</sub>G<sub>3</sub>A<sub>4</sub>A<sub>5</sub>A<sub>6</sub>T<sub>7</sub>T<sub>8</sub>A<sub>9</sub>C<sub>10</sub>C<sub>11</sub>G<sub>12</sub>-3' shown in a front view (a) and rotated 90 degrees around the helix axis. Three DNA-binding modes are observed: (i) metalloinsertion, whereby the ruthenium complex (red) inserts the dppz ligand into the DNA duplex (gray) at the mismatched sites through the minor groove, extruding the mispaired adenosines (blue), (ii) metallointercalation, whereby the complex (green) binds between two well matched base pairs, and (iii) end-capping, whereby the complex (yellow) stacks with the terminal Watson-Crick pair of the duplex.

**Figure 2.**

Two independent views of metalloinsertion at the mismatched sites. a, Superposition of the two independent views of metalloinsertion by the ruthenium complex at the mismatched sites, as viewed from the minor groove (A<sub>4</sub>-A<sub>9</sub> site: ruthenium complex in red and DNA in gray, A<sub>9</sub>-A<sub>4</sub> site: ruthenium complex in green and DNA in blue). The ruthenium complex inserts the dppz ligand from the minor groove and extrudes the mismatched adenosines, which are folded back into the minor groove. The two binding sites were superimposed using only the DNA backbone atoms (rmsd of 42 atoms = 0.607 Å). b, Superimposed metalloinsertion sites as viewed down the helical axis.

**Figure 3.**

Two independent views of metallointercalation at well-matched sites. a, The ruthenium complex intercalates at the 5'-C<sub>1</sub>G<sub>2</sub>-3' step through the dppz ligand (Ru in orange, DNA and bpy from a neighboring ruthenium in blue). b, Metallointercalation at the 5'-A<sub>6</sub>T<sub>7</sub>-3' step (Ru in magenta, DNA in gray).

**Figure 4.**

The end-capping complex. The duplex (dark gray) is end-capped by the ruthenium complex (red), which stacks between an extruded adenosine (blue) and the first complex (yellow) in a crystallographically related duplex (light gray). The last GC base pair (cytidine in cyan and guanosine in green) forms a frayed end.

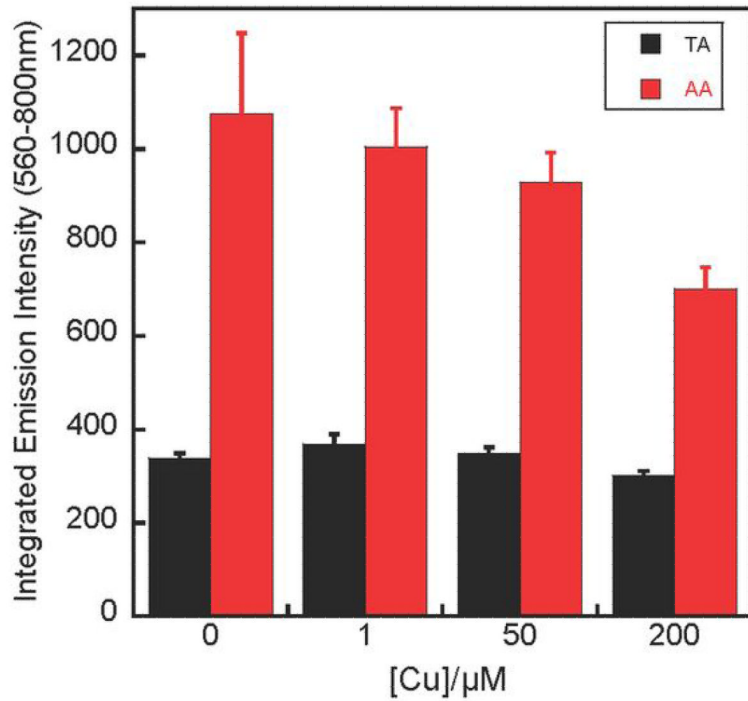


**Figure 5.**

Solution luminescence. Plot of integrated emission intensity ( $\lambda_{\text{ex}} = 440 \text{ nm}$ ) of  $1 \mu\text{M} \Delta\text{-Ru(bpy)}_2\text{dppz}^{2+}$  (1) with increasing concentration of  $\text{Cu}(\text{phen})_2^{2+}$  in the presence of 12-mer mismatched (AA) and well-matched DNA (TA,  $1 \mu\text{M}$ ). Error bars indicate standard deviations in the measurements.

Helical parameters<sup>a</sup> of DNA conformation relating consecutive base pairs.<sup>b</sup>

Step	Ru binding mode	Shift (Å)	Slide (Å)	Rise (Å)	Tilt (°)	Roll (°)	Twist (°)
C <sub>1</sub> /G <sub>2</sub>	intercalation	0.1	2.2	6.3	12.5	5.5	18.1
G <sub>2</sub> /G <sub>3</sub>	-	0.9	0.3	2.9	-3.0	-5.4	30.4
G <sub>3</sub> /A <sub>5</sub>	insertion	0.6	3.5	7.0	5.4	16.6	71.7
A <sub>5</sub> /A <sub>6</sub>	-	-0.8	-0.1	3.0	-0.7	-0.7	23.2
A <sub>6</sub> T <sub>7</sub>	intercalation	-0.2	0.6	7.1	-1.7	7.6	23.5
T <sub>7</sub> T <sub>8</sub>	-	0.4	-0.4	2.8	-3.4	6.6	23.6
T <sub>8</sub> C <sub>10</sub>	insertion	-0.9	3.4	7.3	-7.5	9.0	70.2
C <sub>10</sub> /C <sub>11</sub>	-	-1.0	-0.3	3.0	3.2	-7.5	23.4
B-DNA	-	-0.1	-0.8	3.3	-1.3	-3.6	36

<sup>a</sup>Geometrical relationships between consecutive base pairs: shift, translation into the groove, slide, translation toward the phosphodiester backbone, rise, translation along the helix axis, tilt, rotation about the pseudo-twofold axis relating the DNA strands, roll, rotation about a vector between the C1' atoms, and twist, rotation about the helix axis.

<sup>b</sup>Data were calculated using 3DNA.<sup>41</sup>